

2021

Experimental investigation of pressure drop performance of smooth and dimpled single plate-fin heat exchangers

Kanishk Rauthan
Edith Cowan University

Ferdinando G. Guzzomi
Edith Cowan University

Ana Vafadar
Edith Cowan University

Kevin Hayward
Edith Cowan University

Aakash Hurry
Edith Cowan University

Follow this and additional works at: <https://ro.ecu.edu.au/ecuworkspost2013>



Part of the [Engineering Commons](#)

[10.3390/met11111757](https://doi.org/10.3390/met11111757)

Rauthan, K., Guzzomi, F., Vafadar, A., Hayward, K., & Hurry, A. (2021). Experimental investigation of pressure drop performance of smooth and dimpled single plate-fin heat exchangers. *Metals*, 11(11), article 1757. <https://doi.org/10.3390/met11111757>

This Journal Article is posted at Research Online.
<https://ro.ecu.edu.au/ecuworkspost2013/11425>

Article

Experimental Investigation of Pressure Drop Performance of Smooth and Dimpled Single Plate-Fin Heat Exchangers

Kanishk Rauthan ^{*} , Ferdinando Guzzomi, Ana Vafadar , Kevin Hayward  and Aakash Hurry 

School of Engineering, Edith Cowan University, Joondalup, WA 6027, Australia; f.guzzomi@ecu.edu.au (F.G.); a.vafadarshamasbi@ecu.edu.au (A.V.); Kevin.Hayward@ecu.edu.au (K.H.); a.hurry@ecu.edu.au (A.H.)

* Correspondence: k.rauthan@ecu.edu.au; Tel.: +61-8-6304-4690

Abstract: Passive heat exchangers (HXs) form an inseparable part of the manufacturing industry as they provide high-efficiency cooling at minimal overhead costs. Along with the aspects of high thermal cooling, it is essential to monitor pressure loss while using plate-fin HXs because pressure loss can introduce additional power costs to a system. In this paper, an experimental study was conducted to look at the effects of dimples on the pressure drop characteristics of single plate-fin heat exchangers. To enable this, different configurations of National Advisory Committee for Aeronautics (NACA) fins with smooth surfaces and 2 mm-diameter dimples, 4 mm-diameter dimples and 6 mm-diameter dimples were designed and 3D printed using fused deposition modelling (FDM) of ABS plastic. The depth to diameter ratio for these dimples was kept constant at 0.3 with varied diameters and depths. These were then tested using a subsonic wind tunnel comprised of inlet and outlet pressure taps as well as a hot wire velocimeter. Measurements were taken for pressure differences as well as average velocity. These were then used to calculate friction factor values and to compare the smooth fin to the dimpled fins in relation to their relative pressure drop performance. It was observed that for lower velocities the 4 mm dimples provided minimum pressure drop, with a difference of 58% when compared to smooth fins. At higher velocities, 6 mm dimples increased the pressure drop by approximately 34% when compared to smooth fins. It can also be concluded from the observed data in this study that shallower dimples produce lower pressure drops compared to deeper dimples when the depth to diameter ratio is kept constant. Accordingly, deeper dimples are more effective in providing drag reduction at lower velocities, whereas shallower dimples are more effective for drag reduction at higher velocities.



Citation: Rauthan, K.; Guzzomi, F.; Vafadar, A.; Hayward, K.; Hurry, A. Experimental Investigation of Pressure Drop Performance of Smooth and Dimpled Single Plate-Fin Heat Exchangers. *Metals* **2021**, *11*, 1757. <https://doi.org/10.3390/met11111757>

Academic Editor: Atila Ertas

Received: 1 October 2021

Accepted: 28 October 2021

Published: 1 November 2021

Publisher's Note: MDPI stays neutral with regard to jurisdictional claims in published maps and institutional affiliations.



Copyright: © 2021 by the authors. Licensee MDPI, Basel, Switzerland. This article is an open access article distributed under the terms and conditions of the Creative Commons Attribution (CC BY) license (<https://creativecommons.org/licenses/by/4.0/>).

Keywords: pressure drop; heat exchanger; additive manufacturing; surface textures; dimples; drag reduction

1. Introduction

When discussing heat exchangers (HXs), a primary or direct contact surface is defined as a surface that separates two fluids at different temperatures. As noted by Thulukkanam [1] and Shah and Sekulic [2], additional surfaces can be attached to a primary surface to increase the heat transfer area and further improve the heat transfer characteristics of an HX. These secondary appendages are referred to as fins and aid with convective heat transfer.

With recent advancements in brazing and welding technology, most currently manufactured compact heat exchangers (CHX) and plate-fin heat exchangers (PFHX) involve the brazing, semi-welding and all-welding of plates to a core [3]. Diffusion-bonded HXs have also been applied in high-pressure industrial contexts [4].

Another important development in HX manufacturing is the introduction of additive manufacturing (AM), which allows for complex geometries and matrices to be fabricated [5]. As a result, HXs have become more compact and more efficient [4]. For instance, in a study conducted by Wong et al. [6], it was concluded that an AM-fabricated lattice-structured HX provided minimal resistance to airflow as compared to traditional plate-fin and pin-fin HXs.

However, the presence of a large number of voids within the lattice structure was shown to not allow the adequate transfer of heat, hindering the heat transfer capabilities of the HX. Another example of AM-fabricated HXs is the topology-optimised pin fin heat exchanger that has been developed by Dede, Joshi and Zhou, as shown in Figure 1 [7].

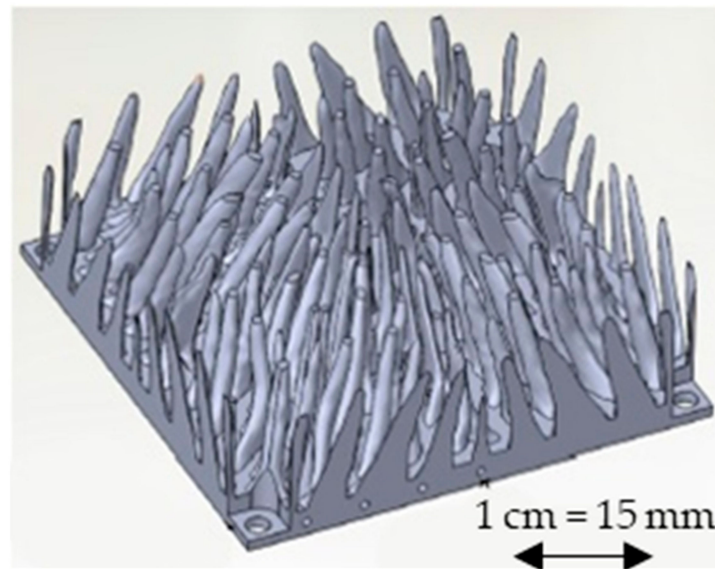


Figure 1. Topology-optimised AM-fabricated Pin-Fin HX CAD model. Reprinted with permission from [7]. Copyright 2015 by American Society of Mechanical Engineers (ASME).

The study conducted by McDonough [8] presents multiple examples of additively manufactured heat exchangers, highlighting the complexity in design along with the ease of fabrication of such complex shapes. Interested readers are highly encouraged to refer to the above-mentioned study to gain in-depth details of applications of additive manufacturing.

Further details of this are presented in a recently published paper by Vafadar et al. [9]. This above study discusses the application of metal AM in the development of complex geometries, for different industries, including the civil, electrical, oil and gas sectors. AM is presented in the above paper as a viable alternative to conventional machining (CM) in terms of reducing both costs and energy consumption [10].

The high thermal performance of CHXs (up to 98%) in combination with an ever-increasing demand for higher rates of heat transfer has prompted the research and development of heat transfer augmentation techniques that have minimal pressure drop penalties via the aid of forced convection. Forced convection, as defined by Sheikholeslami and Ganji [11], refers to the mechanism of fluid transport where fluid is brought into motion using external sources, such as pumps, fans, blowers, etc. To achieve this, there are two methods of heat transfer augmentation that are widely applied in forced convection: using complex shapes and using surface textures on extended surfaces.

One of the most commonly used types of HXs are PFHXs, which have external fins that increase the overall heat transfer area of an exchanger. These fins can be further modified to introduce turbulence in the flow, which enhances heat transfer [12]. These modifications may occur in the form of surface textures that are classified as passive methods of heat transfer enhancement, since they do not require any external source of power. Often, this enhancement in heat transfer is accompanied by an increase in pressure drop that requires additional pumping power for fans/blowers [12]. Hence, investigating surface textures to enhance heat transfer with a reduced pressure drop has become a major area of research for engineers.

Surface textures are an extension of passive methods and include features that are embossed/engraved on the surfaces of HXs to improve thermal and pressure drop per-

performances. One surface texture that has been extensively studied by a range of different researchers is dimples. A number of numerical and experimental studies have been conducted that deal with dimples as a means of improving heat transfer while reducing drag/pressure drop. For instance, Burgess and Ligrani [13] have investigated the effects of dimple depth on the Nusselt number and friction factor, considering the dimple print diameter to dimple depth ratios (ϵ) of 0.1, 0.2 and 0.3 whilst keeping the print diameter constant at 50.8 mm with constant streamwise and spanwise pitches of 82.2 and 41.1 mm, respectively. Streamwise pitch (s) reflects the spacing between the dimples in the direction of the flow, whereas spanwise pitch (p) defines the spacing between dimples perpendicular to the flow of the fluid.

Their study compared the experimental values obtained for a depth to diameter ratio of 0.1 with other studies possessing depth to diameter ratios of 0.2, 0.3, 0.28 and 0.19 for friction factor values. Their study concluded that the values of friction factors increased with either an increase in depth to diameter ratio or an increase in the number of dimples [13]. Investigations conducted by Rao, Wan and Xu [14] on pin-fin dimpled channels with various dimple depths have revealed the dependency of pressure loss behaviour on dimple depth to diameter ratios. Further, their study included dimple depth to diameter ratios of 0.1, 0.2 and 0.3, where the obtained results showed that pin-fin dimple channels with shallower dimples exhibited a reduction of up to 17.6% for the values of friction factors [14]. Experiments on various density patterns of dimples along with different dimple depths have been conducted by Nesselrooij et al. [15] to show the sensitivity of drag reduction to the direction of fluid flow and flow conditions such as the bulk velocity. Their study looked at dimple depths of 0.025 and 0.05 with 20 mm and 60 mm dimple print diameters, respectively. Multiple dimple orientations, such as flow aligned and staggered, were also investigated.

Nesselrooij et al. [15] concluded that for both low-density and high-density patterns, increasing the depth to diameter ratio from 0.025 to 0.05 increased the overall drag at all velocities. The reason for this was attributed to the interactions between the boundary layer and the spanwise velocity component [15]. In turn, shallow dimples with low-density patterns produced a drag coefficient that was 4% less than the drag coefficient for flat plates [15]. Although drag reduction for the high-density deeper dimples improved with the Reynolds number, it still produced an 8% increase in drag performance [15]. Rao and Feng [16] conducted experimental and numerical studies for spherical and teardrop dimples with a depth to diameter ratio of 0.2. Their study concluded that compared to smooth flat plate, both dimple geometries increased the friction factor with the teardrop dimpled channel having relatively higher friction factor values than those of spherical dimples [16].

Moon, O'Connell and Glezer [17] experimentally investigated the effect of the fluid flow channel height on the heat transfer coefficient and friction factor. They tested four different channel heights (6, 13, 19 and 25 mm) while keeping the channel width and length constant. The bottom surface of the test setup was machined to incorporate the dimples.

Their study revealed that heat transfer improved by approximately two-fold, whilst friction factors ranged from 1.6 to 2 times relative to a smooth channel [17]. Moon, O'Connell and Glezer [17] also noted that studies conducted by other authors on dimples showed a lower pressure drop in comparison to other turbulators (such as continuous ribs) whilst significantly improving the thermal performance by a margin of 38%. Several other authors, including Abbas et al. [18], Zhong et al. [19] and Yan, Yang and Wang [20], have also conducted studies on the drag reduction properties of dimples on golf balls and cylinders, concluding that the addition of dimples has a significant effect on reducing the overall drag observed.

It is evident from the above review that much research and many experiments have been conducted using dimpled surfaces on a flat plate. Although flat plates provide a good indication of the thermal and pressure drop performances of dimpled HXs, they do not provide information regarding their implementation for plate-fin compact heat exchangers.

This is due to the difference in the orientation of PFHXs when compared to flat plates. In practical applications of PFHXs, multiple sides of the fins are exposed to the fluid flow and the fins are indeed perpendicular to the flow. Additionally, there is much disparity within the current literature on dimpled channel heat exchangers in terms of results relating to the thermal and pressure drop performances, a gap which the current study seeks to bridge. The effects of variable dimple diameters and dimple depths on the pressure drop performance of single elliptical plate-fin HXs will be tested. These will be compared to experimental results and conclusions provided by various authors. Based on the results of this current study, future work can be conducted on the thermal performances of various dimple configurations.

It should be noted here that the scope of the current study is limited to the investigation of passive surface textures, as they do not require any additional machines or materials to be formed/created. One of these surface modifications makes use of the dimples as turbulators to improve heat transfer while introducing a minimal pressure drop.

2. Experimental Study

2.1. Experimental Setup

For the experimental setup, the 'AF1125 Subsonic Wind Tunnel' (TECQUIPMENT, Nottingham, UK) was utilised, since it is able to replicate forced convection conditions as seen in the real-world applications of PFHXs. The following Figure 2 shows an overview of the experimental setup.

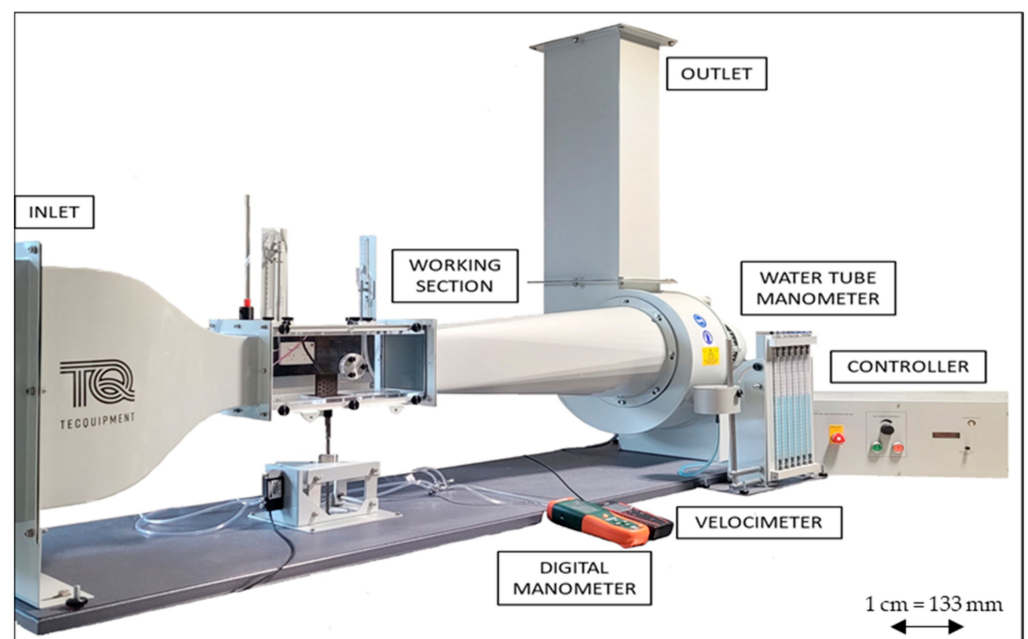


Figure 2. AF1125 subsonic wind tunnel.

The AF1125 wind tunnel consists of an inlet air duct followed by a rectangular working section, a diverging outlet duct and a blower that sits at the end of the diverging duct. The fluid (air) is drawn into the wind tunnel by the blower. Before entering the working section, the fluid encounters the flow straightener which sits right at the entrance of the inlet. The flow straightener minimises the lateral movement of fluid caused by the suction of the fluid and the swirling motion of the air by allowing the air to pass through an array of honeycomb-shaped cells. This ensures that the fluid reaching the working section has no lateral components of velocity and that the flow is as straight as possible.

The rectangular working section measures at a cross section of 125 mm × 125 mm, with a length of 350 mm. Further, it is equipped with four manometer probes that measure the static and dynamic pressure in the inlet and outlet sections of the wind tunnel. Static

pressure or mechanical pressure, as defined by Shaughnessy, Katz and Schaffer [21], is the force measured perpendicular to a surface of interest that is exposed to fluid. This form of pressure represents the average of the normal stress at a certain point within the fluid. Accordingly, if the kinetic energy of a fluid particle was converted into pressure potential energy, the increase in the pressure due to this conversion is represented by dynamic pressure [21]. These probes were used in this study to measure the dynamic pressure at the inlet and outlet of the working section with the aid of HD755 digital differential manometer (EXTECH, Nashua, NH, USA). The manometer measures the pressure difference between two points. Notably, it was connected to measure the difference between the pitot tube pressure and the static pressure values at the inlet and outlet, respectively. Aquarium valves were used to switch between the inlet and outlet pressure taps in this study, as is shown in Figure 3. Pressure values were also used as performance indicators for assessing the pressure drop performances of the varied HXs that were tested. Finally, VT110 velocimeter (KIMO Instruments, Mumbai, India) was installed near the inlet section to measure the velocity of the inlet flow. The measured velocity was then used to calculate the Reynolds number of the free stream flow.

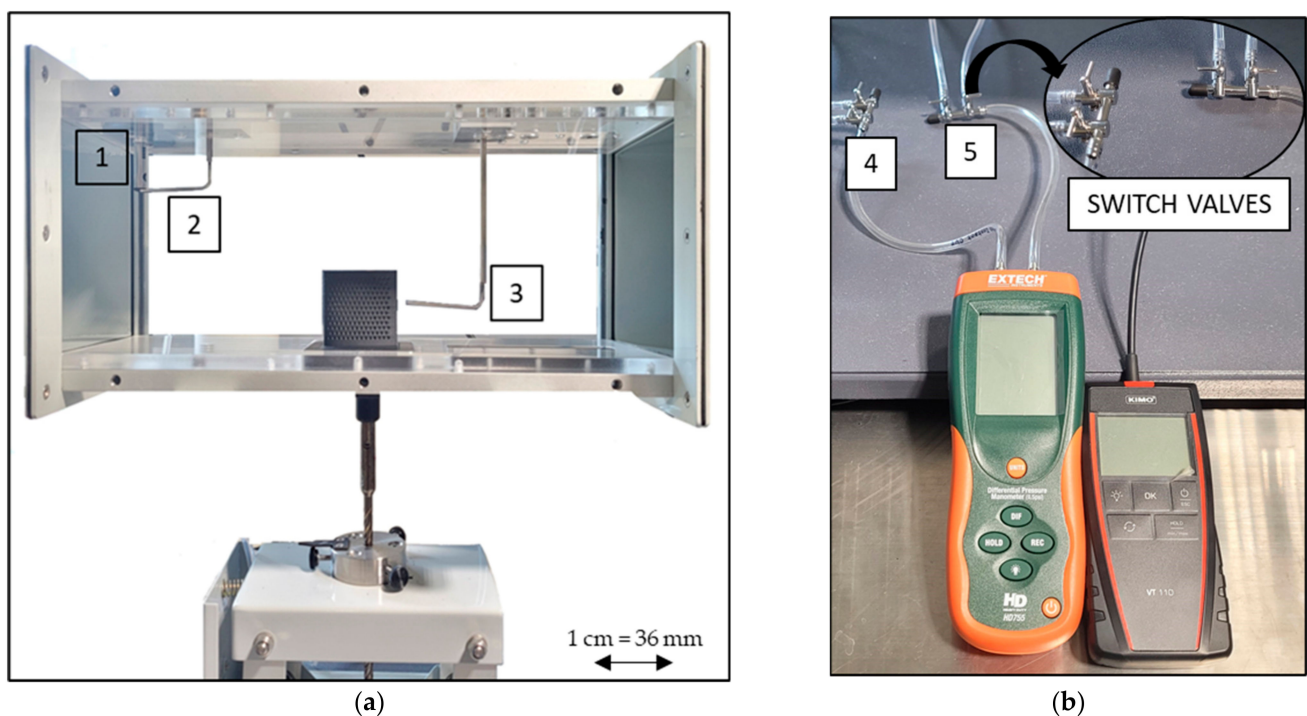


Figure 3. (a) Subsonic wind tunnel working section with the fin; (b) digital manometer and hot wire anemometer together with the switch valve assembly.

Table 1 summarises the apparatus and the various measuring components installed within the wind tunnel, and these are further highlighted in Figure 3.

Table 1. Component list for pressure testing in subsonic wind tunnel.

Sr. No.	Component
1	Velocimeter
2	Inlet Pressure Probes
3	Outlet Pressure Probes
4	Inlet Differential Pressure Valve
5	Outlet Differential Pressure Valve

2.2. Pressure Performance Criteria

There are several parameters that can be used to evaluate the pressure drop performances of heat exchangers, such as the coefficient of drag and friction factor. For the purpose of the current study, friction factor was chosen as the evaluation criteria for pressure drop performance, as measuring the coefficient of drag was not feasible. The experimental setup illustrated in Section 2.1 has been designed specifically to measure the inlet and outlet dynamic pressure, as well as the free stream velocity. Friction factor emerges as the preferred choice in representing the head loss within the test section due to friction, since it is directly proportional to the pressure drop, as shown in Equation (1). Friction factor values allow for results to be presented in a non-dimensional form, which can be readily evaluated against results from similar studies in relation to the coefficient of drag.

2.2.1. Friction Factor

The friction factor or Darcy friction factor can be used to estimate pressure loss due to friction in pipe flow or open-channel flow [22]; it is a non-dimensional quantity and can be expressed using the general equation shown below, adapted from Barker [22].

$$f = \frac{\Delta P 2 D_h}{\rho L V^2} \quad (1)$$

where f is the dimensionless Darcy friction factor, ρ (kg/m^3) is the fluid density, L (m) is the characteristic length of the fin, V (m/s) is the fluid velocity, D_h (m) is the hydraulic diameter and ΔP (Pa) is the pressure difference between the inlet and the outlet of the working section.

The hydraulic diameter can be calculated using the equation given below, which has been adapted from Genium Publishing Corporation [23].

$$D_h = \frac{2WH}{(H + W)} \quad (2)$$

where W (m) and H (m) are the width and height of the wind tunnel working section, respectively.

2.2.2. Reynolds Number

The Reynolds number can be used to characterise the inertial and viscous properties of a moving fluid [24], where it can be calculated using the equation given below that has been adapted from Vafadar, Guzzomi and Hayward [25].

$$Re = \frac{\rho V D_h}{\mu} \quad (3)$$

where μ ($\text{kg}/\text{m}\cdot\text{s}$) is the dynamic viscosity of the fluid.

2.3. Uncertainty

Since the results are presented relatively using the same exact test equipment, uncertainty was calculated using single sample standard deviation in order to outline inaccuracies in measurements and to describe the reliability of the results. Standard deviation was calculated for the 5 individual runs to make sure the experimental data and the equipment did not show any error. A maximum standard deviation of 8% was noted for the smooth NACA fin at a velocity of 12 m/s. Standard deviation for the remainder of the tests was below 5%. These uncertainties are within a reasonable range of accuracy, where similar uncertainties have been noted by Burgess and Ligrani [13] as well as Rao, Li and Feng [16]. Individual runs for all geometry profiles were conducted consecutively within a period of 120 min. This was to ensure the ambient conditions within the lab were as consistent as possible for all individual runs, without introducing bias from external factors such as change in temperature, pressure and humidity.

2.4. Test Methodology

Thermal probes were removed from within the test section to avoid hindering the path of the fluid and to ensure the pressure drop was based solely on the geometry being tested. The bottom section of the wind tunnel was redesigned in a way to accommodate the base of the fin and to make it flush with the bottom panel of the wind tunnel. In turn, this excludes the pressure drop of the plate itself and provides measurements for only the pressure drop performance of the fin and the dimples.

Pilot tests were conducted to establish the range of velocities to be tested, where velocities from 2 m/s to 30 m/s were tested. Since the range of the velocimeter reached its maximum at 30 m/s, pressure readings were measured at velocities starting at 12 m/s and going up in increments of 2 m/s thereafter until 28 m/s. This made it possible to obtain nine measurements to evaluate the pressure drop. Pressure measurements at 30 m/s were not measured since the velocimeter failed to provide consistent readings, where subsequent experimental data showed a relatively large standard deviation. Similarly, velocities below 12 m/s showed inconsistent pressure readings for the NACA fins and therefore, were not included in these tests. The main reason for this inconsistency in the measurements was the limited range of the measuring equipment which failed to provide adequate measurements for velocities below 12 m/s and beyond 28 m/s.

Experiments were conducted five times for each of the geometries being tested. Initially, ten pilot tests were conducted, where standard deviation was calculated for five runs and ten runs, respectively. Average standard deviations of 0.29 Pa and 0.27 Pa were observed for the five and ten runs, respectively. Accordingly, it was decided that five runs were sufficient to ensure accurate results without increasing the uncertainty of the measurements. An average of the five collective runs was used for the final calculation of friction factor as well as Reynolds number.

During the experiments, static inlet/outlet pressure, dynamic inlet/outlet pressure, ambient room temperature and fluid velocity were recorded. These were further used to calculate friction factor for different fin geometries.

A boundary layer thickness of 3 mm was estimated based on flat plate approximation of the elliptical fin along the length of the entire NACA profile. As a result, the pitot tube within the wake/outlet section of the fin was positioned 6 mm off the trailing edge of the fin in order to not capture the boundary layer effects and measure the pressure drop based on the wake of the fin. An equation suggested by Çengel and Cimbala [26] was used to calculate the approximate thickness of the turbulent boundary layer based on flat plate approximation.

$$\delta \approx x \times \frac{0.38}{(Re)^{1/5}} \quad (4)$$

where δ is the boundary layer thickness (mm), x is the characteristic length from the leading edge (mm) and Re is the Reynolds number (dimensionless).

A digital manometer was used to provide a rolling average of the pressure drop for the inlet and outlet sections of the tested fins. Similarly, a velocimeter was used at the inlet section to calculate the average of the velocity. Both the manometer and velocimeter do not have the capability to provide values over a data acquisition system, whereby the rolling average was taken for the pressure and velocity. The overall pressure drop was then calculated by obtaining the difference between the inlet and outlet's averaged experimental pressure values, whilst the Reynolds number was calculated using the average of the velocity distribution.

2.5. Test Parameters

Different configurations of dimples, as shown in Figure 4, were tested. The aim was to investigate the effect of varying dimple diameters and depths on pressure drop performance while keeping the depth to diameter ratio, also known as surface roughness (ϵ), constant at 0.3.

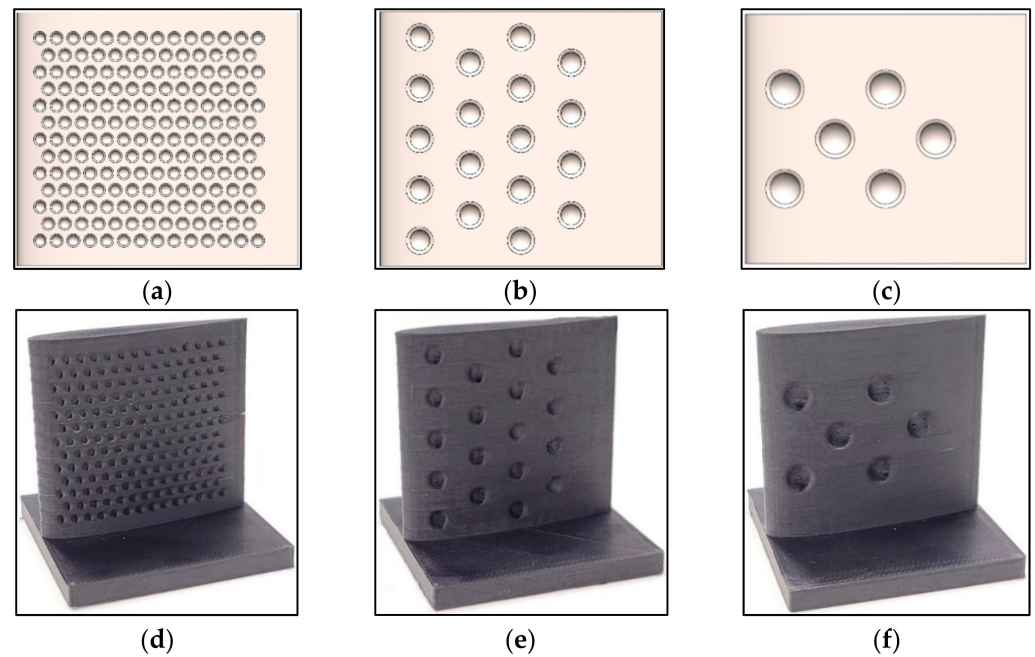


Figure 4. (a) HX 1–2 mm dimples; (b) HX 2–4 mm dimples; (c) HX 3–6 mm dimples; (d) 3D-printed HX 1; (e) 3D-printed HX 2; (f) 3D-printed HX 3.

Test fins were fabricated using 3D printing of ABS plastic with Zortrax M200 3D printer (Zortrax, Olsztyn, Poland). Three-dimensional models were developed for the plate and the fin as a single solid using Solidworks (Dassault Systèmes, Waltham, MA, USA) and these were then converted into appropriate file formats to process using the Zortrax M200 (Zortrax, Olsztyn, Poland). Three-dimensional-printed fins were then inspected for surface defects and irregularities. No post-processing of the fins was required and the finished samples are shown below in Figure 4.

Initial experiments investigated the effects of varying the dimple diameter and depth on pressure drop performance; the tested dimple geometries are shown in Figure 4.

These dimpled fins' pressure drop performances were compared to the smooth NACA 63-015 profile fin. Measurements for the smooth fin were used as the base measurements to indicate the effective change in pressure drop after implementing dimples. The smooth fin is shown below in Figure 5.

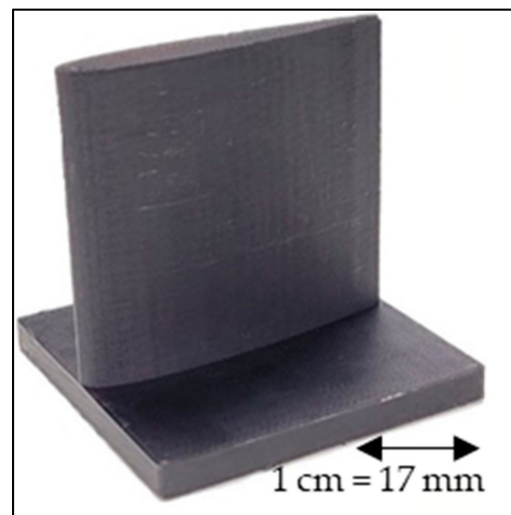


Figure 5. NACA 63-015-inspired smooth 3D-printed PFHX.

As stated in the literature review, a larger diameter to depth ratio has been shown/proven to provide a better thermal performance. A large diameter to depth ratio can introduce stagnant air pockets and turbulence, which may increase the pressure drop. Therefore, dimple diameters of 2 mm, 4 mm and 6 mm were chosen with a D/d ratio of 0.3. The selection of the ratio was based upon the previous studies while the selection of the dimple diameters was limited by the geometry of the fin and the manufacturing equipment. All fins were printed using the Zortrax M200 3D printer which provides a resolution of 0.4 mm for a single printable point. Taking this into consideration and the curvature of the dimples, it was decided to use 2 mm as the minimum dimple size which corresponds to a depth of 0.6 mm. Dimple diameters lower than 2 mm would have depths lower than 0.4 mm, which when manufactured would lose the details of the curvature of the dimple. The number of dimples on the fins for the above-mentioned diameters were 352, 36 and 12, respectively. The number and configuration of dimples were normalised using the volume of material removed, where all efforts were made to keep the removed volume as consistent as possible. This is shown in Table 2.

Table 2. Smooth vs. dimpled fins' mechanical properties.

Fin	Fin Volume (mm ³)	Fin Surface Area (mm ²)	Δ Volume (mm ³)	Δ S.A (mm ²)
HX Smooth	11,571	5149	-	-
HX 1–2 mm Dimples	11,191	5475	380	326
HX 2–4 mm Dimples	11,260	5277	311	128
HX 3–6 mm Dimples	11,216	5241	356	91

Figure 6a,b present the geometrical dimensions used to create the varied dimple profile and the array of dimples on the fin, respectively.

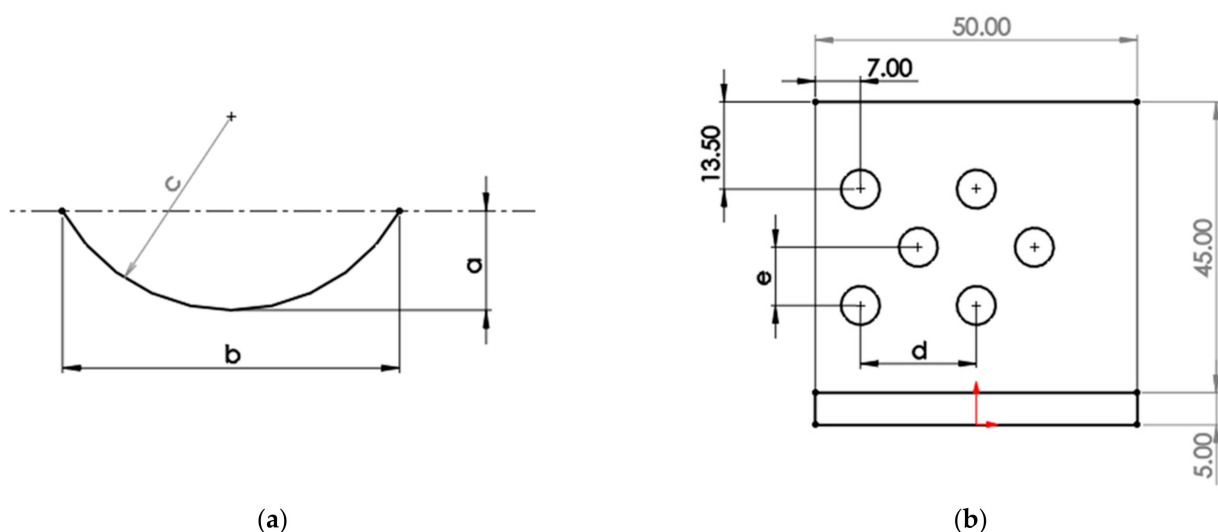


Figure 6. Geometrical dimensions for (a) dimple profile; (b) fin with dimples. Dimensions are in millimeters (mm).

Table 3 below presents the summary of the samples that were tested in the current study, including the geometrical configurations of dimples as well as their span-wise/streamwise spacing. All dimensions are in millimeters.

Table 3. Geometric configuration of HX samples.

Fin	a	b	c	d	e	a/b
HX Smooth	-	-	-	-	-	-
HX 1–2 mm Dimples	0.6	2	1.13	3	3	0.3
HX 2–4 mm Dimples	1.2	4	2.27	18	4.5	0.3
HX 3–6 mm Dimples	1.8	6	3.4	18	9	0.3

3. Results

Figure 7a presents the average of the pressure drop measurements for the smooth NACA 63-015 fin whereas Figure 7b shows the results of five individual runs that were undertaken for the NACA fin. The trendline corresponds to a second-order polynomial equation, the coefficient for which is shown in Figure 7a.

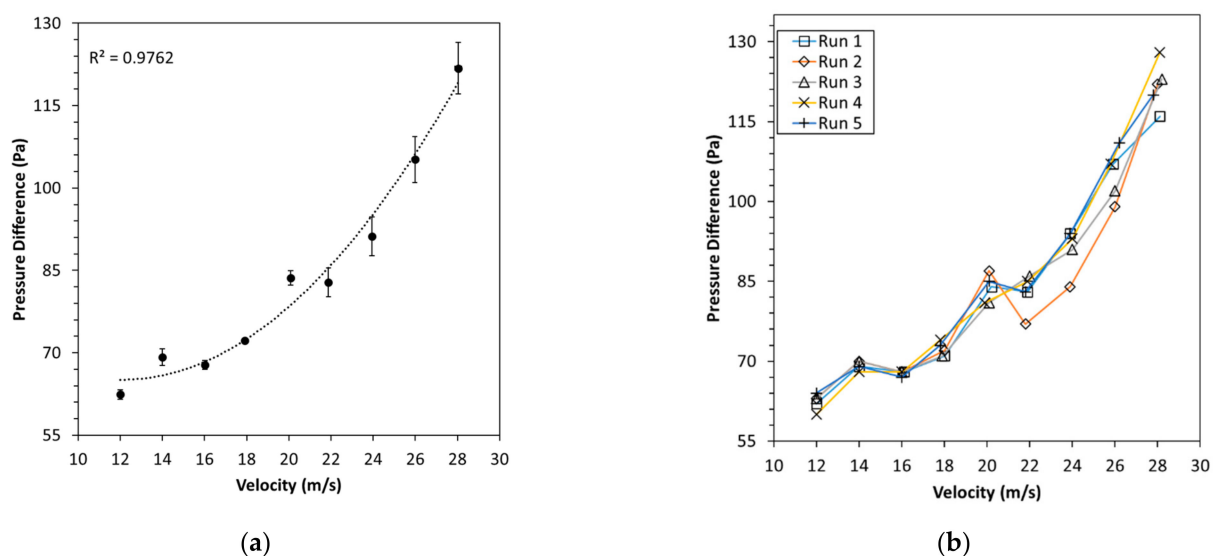


Figure 7. Experimental results for smooth NACA/elliptical profile; (a) average of 5 runs and (b) 5 individual runs.

Figure 8a presents the average of the pressure drop measurements for the 2 mm-dimpled fin whereas Figure 8b provides the pressure measurements for the five individual runs. The trendline corresponds to a second-order polynomial equation, the coefficient for which is shown in Figure 8a.

Figure 9a shows the pressure drop measurements for the 4 mm-dimpled fin and Figure 9b provides the results for the five individual measurements undertaken. The trendline corresponds to a second-order polynomial equation, the coefficient for which is shown in Figure 9a.

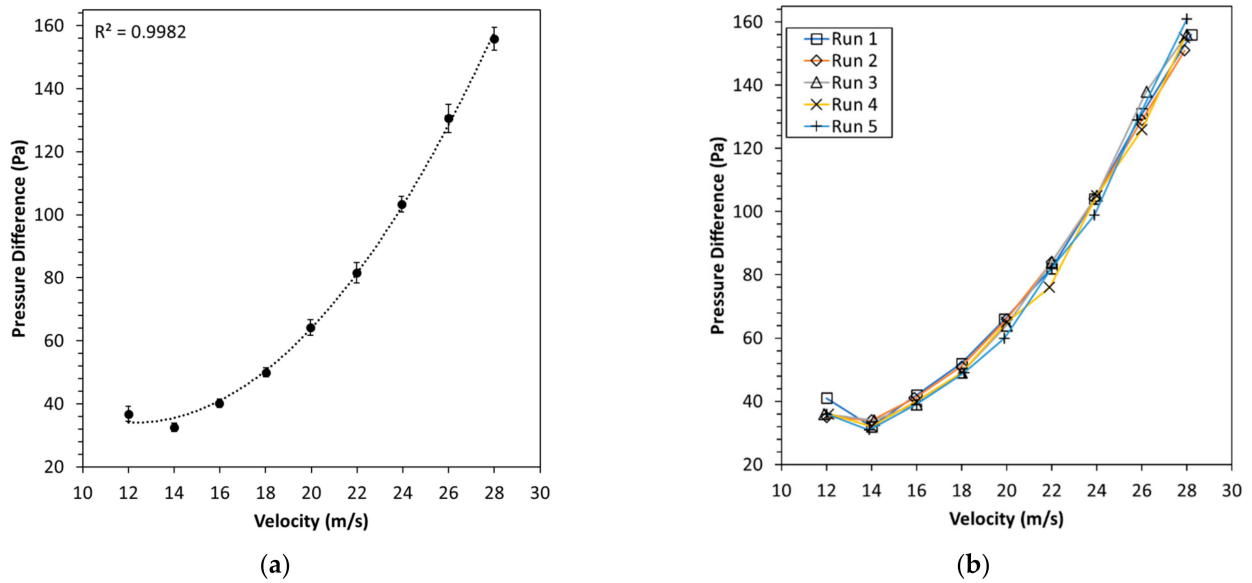


Figure 8. Experimental results for 2 mm dimples engraved on the NACA/elliptical Profile; (a) average of 5 runs; (b) 5 individual runs.

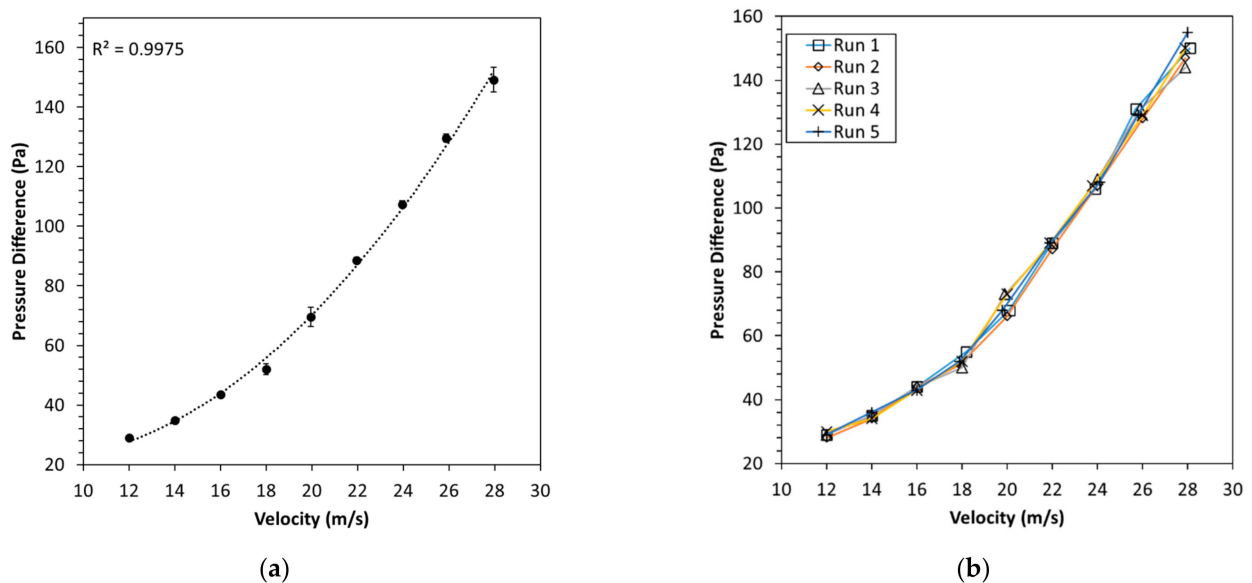


Figure 9. Experimental results for 4 mm dimples engraved on NACA/elliptical profile; (a) average of 5 runs; (b) 5 individual runs.

Figure 10a highlights the average pressure drop for the 6 mm-dimpled fin whereas Figure 10b presents the results for the five individual runs undertaken. The trendline corresponds to a second-order polynomial equation, the coefficient for which is shown in Figure 10a.

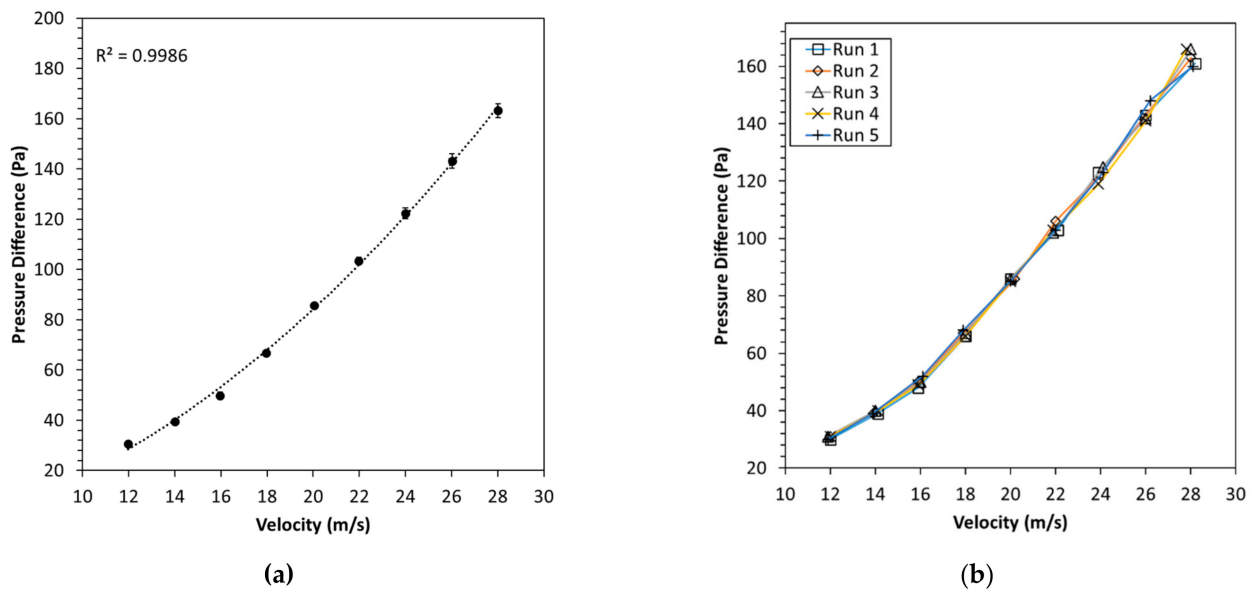


Figure 10. Experimental results for 6 mm dimples engraved on NACA/elliptical profile; (a) average of 5 runs; (b) 5 individual runs.

Figures 11 and 12 compares the pressure drop performances of the different dimpled fins (2 mm, 4 mm, 6 mm) against the smooth NACA fin as well as their friction factor characteristics.

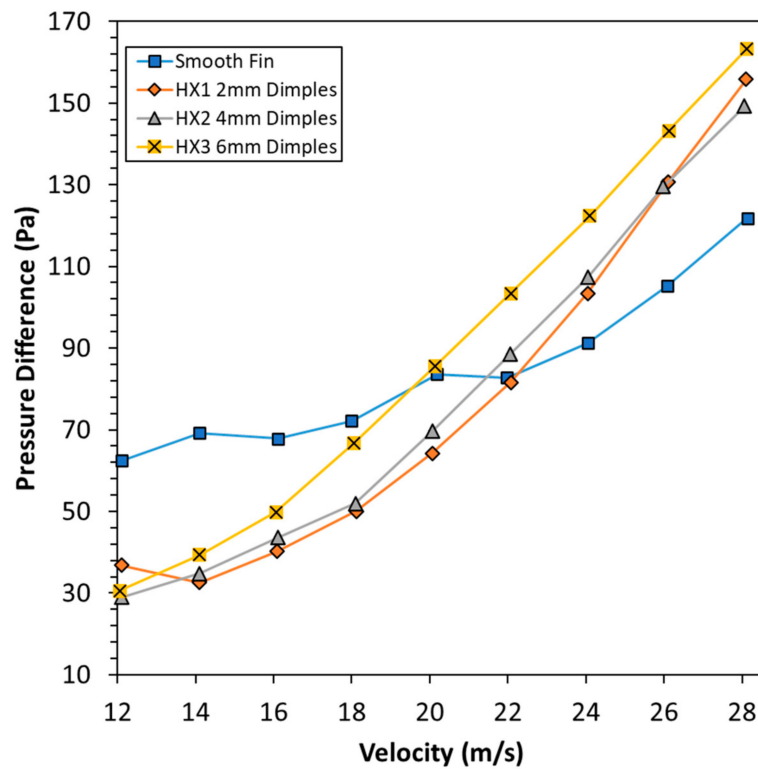


Figure 11. Comparison of pressure drop between smooth, 2 mm, 4 mm and 6 mm dimples engraved on NACA/elliptical profile.

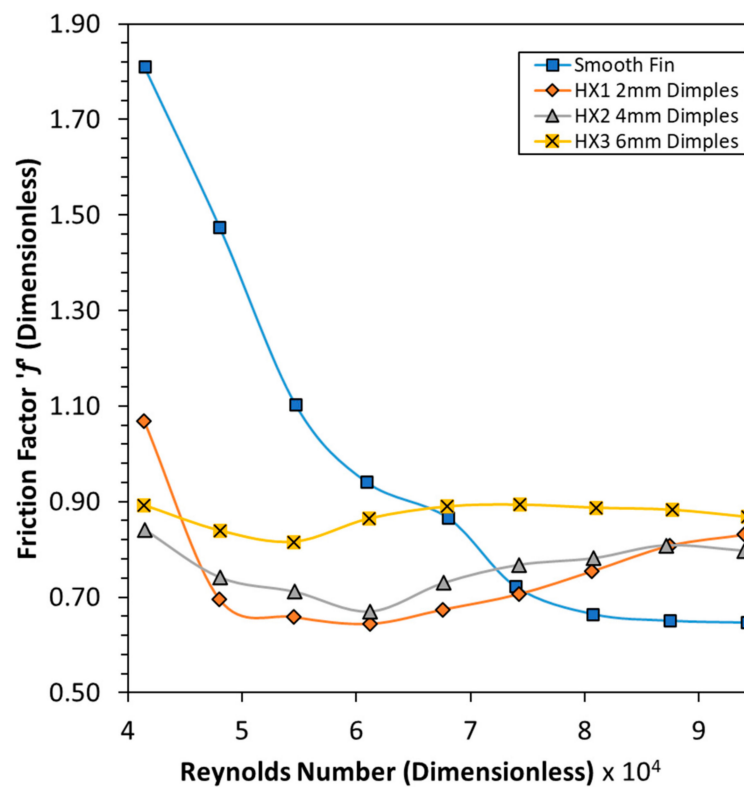


Figure 12. Comparison of friction factor value between smooth, 2 mm, 4 mm and 6 mm dimples engraved on NACA/elliptical profile.

4. Discussion of Results

The results from the wind tunnel testing of smooth NACA/elliptical fin, and fins with 2 mm, 4 mm and 6 mm dimples, are presented in Figure 7, Figure 8, Figure 9, Figure 10, respectively. These include the five individual runs to determine the accuracy of the measurement as well as the average of these five runs. These average runs were then compared to each other, as seen in in Figure 11, for their relative pressure drop performances. It can be observed in Figure 11 that with an increase in diameter as well as depth of the dimples, there was a noticeable increase in the pressure drop of the fins. A similar trend has been observed by Ting [27] in relation to golf balls, where initially increasing the surface roughness of golf balls via dimples reduced the coefficient of drag. The above study also observed that after a certain limit is reached for dimple depth, a further increase in the depth of dimples had the opposite effect, where the coefficient of drag increased significantly. In the current study, fins with dimples outperformed the smooth fin in terms of pressure drop performance up to velocities of 20 m/s, after which the pressure drop for the dimpled fins increased significantly. These observations can be attributed to the fact that the addition of dimples delays the boundary layer separation, which subsequently induces a narrower wake behind the fin leading to reduced form drag. These dimples introduce localised turbulence within and around the dimple cavity, which re-energizes the boundary layer and delays boundary layer separation. As a result of this localised turbulence, the boundary layer sticks to the surface for a longer duration and reduces the overall wake behind the fin. This contributes to a reduction in form drag, which is seen as the initial decline in the friction factor or the lower pressure drop observed with a low Reynolds number. Form drag is highly dependent on flow separation, whereas friction drag is a function of shear stresses observed on the surface of a geometry [28]. With an increase in the Reynolds number, there is an increase in shear stresses, which in turn increases the overall friction drag. For the case of dimpled fins, shear stresses are further magnified due to the introduction of localised turbulence by dimples, where as a result there is a significant increase

in the pressure drop for dimpled fins starting at a velocity of 20–22 m/s, which is equivalent to a Reynolds number of approximately 7×10^4 – 7.5×10^4 . Experiments conducted by Chowdhury et al. [29] have shown that increasing the depth of dimples lowers the critical Reynolds number, where the transition to turbulent flow happens earlier within the flow in comparison to smooth fins. Even though this shift in transition has the possibility of increasing the coefficient of drag in the transcritical regime, as observed by Chowdhury et al. [29], it also creates local turbulence within dimples. This local turbulence can be controlled via the depth of the dimples and used to energise the boundary layer, which delays the aforementioned separation. Accordingly, as can be observed in Figure 11, the fin with 2 mm dimples showed a higher pressure drop at 12 m/s relative to 4 mm and 6 mm dimples, both of which experienced negligible differences in the pressure drop performance at 12 m/s. Starting at 14 m/s, the fin with 2 mm dimples showed a consistently lower pressure drop, followed by fins with 4 mm and 6 mm dimples, respectively. This trend could be observed up until 26 m/s, after which the fin with 2 mm dimples surpassed the 4 mm-dimpled fin and showed an increase in pressure drop. It is worth noting here that the difference in pressure drop between 2 mm- and 4 mm-dimpled fins was quite insignificant when compared with 6 mm dimples. As suggested by various authors, including Ge, Fang and Liu [30], this could be attributed to the threshold of dimple depth and diameter, whereby if the depth and diameter of dimples is increased beyond a limit, the favourable effect of pressure reduction is negated and an increase in pressure drop can consequently be observed.

Figure 12 shows the friction factor calculated using Equation (1) provided in the theory section. The friction factor allows for the comparison of head loss within an open-channel flow, where flow can be observed in a pipe measured over a specific distance [31]. In this study, friction factor values were plotted against the Reynolds number for a smooth fin and dimpled fins (2 mm, 4 mm and 6 mm). This allowed the authors to determine the relationship between the head loss observed within the wind tunnel for various dimpled and non-dimpled fins relative to the Reynolds number. It is evident from the trends observed in Figure 12 that the friction factor for the smooth NACA fin was the highest up to a Reynolds number of 6.5×10^4 , whereas the 2 mm dimples provided the lowest friction factor for Reynolds numbers ranging from 4.6×10^4 to 7.2×10^4 . Experiments conducted by Choi, Jeon and Choi [32] found that with an increase in the Reynolds number, a sharp decrease in the coefficient of drag can be observed for dimpled spheres as compared to smooth spheres. A similar trend is also visible in Figure 12 for the 2 mm-dimpled fin and the smooth fin, where a sharp decrease in the friction factor can be observed for the 2 mm-dimpled fin between Reynolds numbers of 4×10^4 and 5×10^4 , and for the smooth fin between the range of 4×10^4 and 6×10^4 . The same study by Choi, Jeon and Choi [32] further concluded that the coefficient of drag hit a constant value after the sharp decline region. Their study examined dimpled spheres with varied surface roughness values (ϵ), with a higher surface roughness indicating deeper dimples. The results published in the above study further summarised that the coefficient of drag for higher surface roughness (ϵ) spheres showed a sharp decline at a lower Reynolds number while maintaining a higher constant value than spheres with lower surface roughness values (ϵ). Similar observations are evident in Figure 12 where, on the one hand, the equipment could not capture the sharp decline of the friction factor for deeper dimples (4 mm and 6 mm), as was observed for the 2 mm-dimpled fin and the smooth fin. On the other hand, it can be clearly observed that the friction factor starts to plateau at a Reynolds number of approximately 6.8×10^4 , with 6 mm dimples showing the largest head loss, and 2 mm dimples exhibiting the lowest head loss. The overall trend for the coefficient of drag as observed by Choi, Jeon and Choi [32] in their experimental studies can also be observed in Figure 12 for the plot of the friction factor. This similarity in the overall trend can be explained by the formation of a separation bubble within the dimples resulting in delayed boundary layer separation, as mentioned earlier, leading to a reduction in the overall drag and consequently reducing the overall pressure drop.

These results also coincide with the trends observed by Rao, Wan and Xu [14], Nesselrooij et al. [15] and Patel and Borse [33] where the introduction of dimples was shown to reduce pressure drop relative to a flat plate. Further, a study conducted by Rao, Wan and Xu [14] also concluded that shallower dimples perform better at reducing the pressure drop as compared to deeper dimples, since shallower dimples reduce the velocity near the upstream half of the dimples which consequently reduces turbulent mixing in the main flow. With deeper dimples, even though turbulent mixing is reduced in the upstream half of the dimples, there is a strong flow impingement near the downstream rim of the dimples [14]. Interested readers may refer to the above-mentioned study by Rao, Wan and Xu [14] for additional insight regarding the pressure loss due to flow impingement.

This flow impingement introduces additional pressure loss within the flow. This is visible in Figure 11, where the fin with 2 mm dimples provided the lowest pressure drop, followed by fins with 4 mm and 6 mm dimples, respectively. At low velocities of up to 22 m/s, a maximum pressure drop reduction of 58% was observed using 4 mm dimples relative to the smooth NACA fin, whereas at high velocities above 22 m/s, a 34% increase in pressure drop was observed with 6 mm dimples relative to the smooth NACA fin. Figure 13 presents the percentage difference in pressure for all three configurations of dimples tested against the smooth fin.

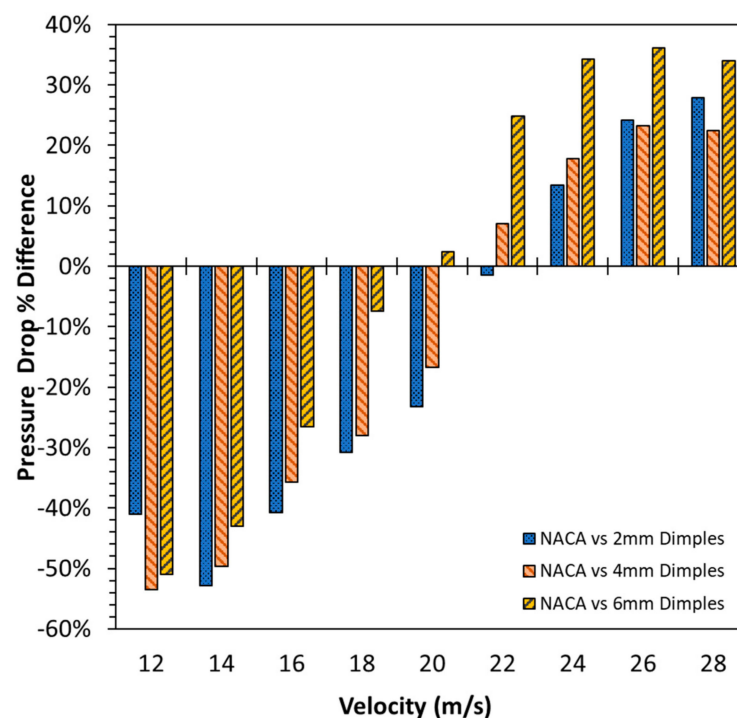


Figure 13. Pressure drop % difference for NACA fin vs. 2 mm-, 4 mm- and 6 mm-dimpled fins.

It should be observed here that the results obtained by several authors including Choi, Jeon and Choi [32] as well as Abbas et al. [18] for drag coefficients coincide with the trends observed in Figure 12 for friction factor values. As a result, it can be summarised from Figure 12 that deeper dimples induce drag reduction at a lower Reynolds number, which can be seen in the sharp decline in the friction factor value for 2 mm dimples. This sudden decrease in friction factor could not be captured in the 4 mm and 6 mm dimples due to the limit of the measuring equipment and the reasons outlined in Section 2.4 of the current study. However, from the similarity of the trends observed in the literature and Figure 12, the critical regime of the sudden decrease in drag for 4 mm and 6 mm dimples should lie beyond a Reynolds number $<4 \times 10^4$. This is evident from the values for a friction factor of 4 mm- and 6 mm-dimpled fins, as they are observed to increase when going from a Reynolds number of 5×10^4 to 4×10^4 , suggesting a linear increase in overall drag at velocities lower

than 12 m/s. Consequently, it can also be concluded from Figure 12 that deeper dimples induce a higher pressure drop at a higher Reynolds number of $>7 \times 10^4$ when compared to shallower dimples. This is evident from the trend where friction factor values start to plateau within the transcritical regime (Re , 6.5×10^4 – 9×10^4), whereby at that stage the 6 mm dimpled fins have the highest friction factor values, followed by the 4 mm- and 2 mm-dimpled fins. The smooth NACA fin provided the lowest frictional resistance. In summary, it is apparent that deeper dimples are preferred for reducing drag at lower velocities with a larger pressure drop in the transcritical regime. Shallower dimples are preferred for medium to high velocities with a smaller pressure drop in the transcritical regime.

5. Conclusions

In this study, we have experimentally investigated the pressure drop characteristics of NACA/elliptical fins with smooth surfaces and with 2 mm, 4 mm and 6 mm engraved dimples. The experimental results for the smooth and dimpled fins were obtained using wind tunnel testing and compared relative to each other for velocities ranging from 12 m/s to 28 m/s, translating to a Reynolds number range of 4×10^4 – 9.2×10^4 . The results show a clear distinction in pressure drop and friction factor for smooth and dimpled fins. Dimpled fins outperformed the smooth fin for velocities of 12 m/s to approximately 22 m/s, with 2 mm-dimpled fins providing the lowest pressure drop and the least friction amongst the compared fins. Another important observation was the increase in the pressure drop and friction factor with relative increases in the dimple diameter and depth. With the depth to diameter ratio being constant at 0.3 for all dimpled fins, it was evident that shallower dimples performed better and induced a lower pressure drop compared to dimples with larger diameters and depths. Dimples with 4 mm diameters led to a reduction of 58% in pressure drop at a velocity of 12 m/s when compared to the smooth fins. Dimples with 2 mm diameters showed a 53% reduction in pressure drop at a velocity of 16 m/s relative to the smooth fin. Dimples with the largest diameter of 6 mm showed a reduction of 55% at a velocity of 12 m/s when compared to the smooth fin and the 2 mm dimples. This occurred due to the fact that a higher surface roughness or deeper dimples shift the critical Reynolds number upstream, which reduces the drag at low velocities while the constant value of the drag coefficient within the transcritical regime increased significantly. A smaller surface roughness or shallower dimples provided a larger drag reduction at higher velocities with the constant value of drag coefficient within the transcritical regime being lower when compared to deeper dimples. As a result, applications that require drag reduction at lower velocities should opt for deeper dimples, whilst applications that require significant drag reduction at high velocities should utilise shallower dimples.

Future Work

The current study focuses on the investigation of the pressure drop characteristics of dimpled fins relative to a smooth NACA fin. Even though favourable results have been obtained with the use of dimples to reduce the pressure drop, a framework is still missing in order to optimise dimple design for specific applications. As a result of the current investigation, the following future works are proposed, which seek to further establish dimples and the use of turbulators as a means of increasing the efficiency of PFHXs.

- Heat transfer studies should be conducted on the geometries investigated in the current study. Even though a significant pressure drop reduction was observed with the introduction of dimples, how well these dimples allowed the transfer of heat will eventually be a decisive factor in the relevance of the use of additive manufacturing and the use of turbulators in improving the efficiency of HXs.
- Mathematical models should be investigated that allow the design of dimples based on common parameters observed in the application of HXs. These include velocity, drag, Reynolds number, surface roughness and other factors that contribute to increasing the pressure drop efficiency of HXs. The current literature regarding dimples has mainly focused on experimental results, where the design of the dimples is either cho-

sen arbitrarily based on existing literature or is influenced by their existing applications in golf balls. These designs have been verified for their effectiveness based on these experimental parameters. A framework or a mathematical model that provides insight into the design of dimple parameters, such as the optimal depth and diameter for specific velocities or specialised applications, will be highly advantageous in removing the need for extensive testing of various arbitrarily chosen dimple designs.

Author Contributions: Conceptualization, A.V., F.G. and K.H.; Methodology, K.R. and A.H.; Investigation, K.R.; Resources, A.V. and F.G.; Data curation, K.R.; Writing—original draft preparation, K.R.; Writing—review and editing, K.R., A.V., F.G., K.H. and A.H.; Supervision, F.G., A.V. and K.H.; Project administration, K.R., F.G., A.V., K.H. and A.H.; Funding acquisition, F.G. and A.V. All authors have read and agreed to the published version of the manuscript.

Funding: This study was supported by Edith Cowan University (ECU) under Grant G1004423. Additionally this manuscript received an open access publication grant from the School of Engineering, Edith Cowan University, Australia.

Institutional Review Board Statement: Not applicable.

Informed Consent Statement: Not applicable.

Data Availability Statement: Not applicable.

Acknowledgments: The authors would like to acknowledge and thank the School of Engineering, Edith Cowan University, Australia, for providing and administering the resources and the requirements for the successful completion of this research. The authors would also like to thank the technical and literacy staff including Adrian Davis, Guanliang Zhou, Yatt Yap and Michael Stein for their support during the course of the research in technical needs and writing requirements.

Conflicts of Interest: The authors declare that there is no conflict of interest.

References

1. Thulukkanam, K. *Heat Exchanger Design Handbook*; Taylor & Francis Group: Boca Raton, FL, USA, 2013.
2. Shah, R.K.; Sekulic, D.P. *Fundamentals of Heat Exchanger Design*; John Wiley & Sons: Hoboken, NJ, USA, 2003.
3. Li, Q.; Flamant, G.; Yuan, X.; Neveu, P.; Luo, L. Compact heat exchangers: A review and future applications for a new generation of high temperature solar receivers. *Renew. Sustain. Energy Rev.* **2011**, *15*, 4855–4875. [[CrossRef](#)]
4. Hesselgreaves, J.E.; Law, R.; Reay, D.A. *Compact Heat Exchangers*; Elsevier: Oxford, UK, 2017.
5. Oliveira, J.P.; LaLonde, A.; Ma, J. Processing parameters in laser powder bed fusion metal additive manufacturing. *Mater. Des.* **2020**, *193*, 108762. [[CrossRef](#)]
6. Wong, M.; Owen, I.; Sutcliffe, C.J.; Puri, A. Convective heat transfer and pressure losses across novel heat sinks fabricated by selective laser melting. *Int. J. Heat Mass Transf.* **2009**, *52*, 281–288. [[CrossRef](#)]
7. Dede, E.M.; Joshi, S.N.; Zhou, F. Topology Optimization, Additive Layer Manufacturing, and Experimental Testing of an Air-Cooled Heat Sink. *J. Mech. Des.* **2015**, *137*, 111403. [[CrossRef](#)]
8. McDonough, J.R. A perspective on the current and future roles of additive manufacturing in process engineering, with an emphasis on heat transfer. *Therm. Sci. Eng. Prog.* **2020**, *19*, 100594. [[CrossRef](#)]
9. Vafadar, A.; Guzzomi, F.; Rassau, A.; Hayward, K. Advances in Metal Additive Manufacturing: A Review of Common Processes, Industrial Applications, and Current Challenges. *Appl. Sci.* **2021**, *11*, 1213. [[CrossRef](#)]
10. Frazier, W.E. Metal Additive Manufacturing: A Review. *J. Mater. Eng. Perform.* **2014**, *23*, 1917–1928. [[CrossRef](#)]
11. Sheikholeslami, M.; Ganji, D.D. Nanofluid Forced Convection Heat Transfer. In *Applications of Nanofluid for Heat Transfer Enhancement*; Elsevier: Amsterdam, The Netherlands, 2017; pp. 127–193.
12. Alam, T.; Kim, M.H. A comprehensive review on single phase heat transfer enhancement techniques in heat exchanger applications. *Renew. Sustain. Energy Rev.* **2018**, *81*, 813–839. [[CrossRef](#)]
13. Burgess, N.; Ligrani, P. Effects of dimple depth on channel nusselt numbers and friction factors. *J. Heat Transf.* **2005**, *127*, 839–847. [[CrossRef](#)]
14. Rao, Y.; Wan, C.; Xu, Y. An experimental study of pressure loss and heat transfer in the pin fin-dimple channels with various dimple depths. *Int. J. Heat Mass Transf.* **2012**, *55*, 6723–6733. [[CrossRef](#)]
15. van Nesselrooij, M.; Veldhuis, L.L.M.; van Oudheusden, B.W.; Schrijer, F.F.J. Drag reduction by means of dimpled surfaces in turbulent boundary layers. *Exp. Fluids* **2016**, *57*, 142. [[CrossRef](#)]
16. Rao, Y.; Li, B.; Feng, Y. Heat transfer of turbulent flow over surfaces with spherical dimples and teardrop dimples. *Exp. Therm. Fluid Sci.* **2015**, *61*, 201–209. [[CrossRef](#)]
17. Moon, H.; O’Connell, T.; Glezer, B. Channel height effect on heat transfer and friction in a dimple passage. *J. Eng. Gas Turbines Power* **2000**, *122*, 307–313. [[CrossRef](#)]

18. Abbas, Z.; Shah, S.I.A.; Javed, A.; Jami, M.L. Influence of dimple design on aerodynamic drag of Golf balls. In Proceedings of the 2019 Sixth International Conference on Aerospace Science and Engineering (ICASE), Islamabad, Pakistan, 12–14 November 2019.
19. Zhong, X.; Shuzhao, L.; Xiaoyan, W.; Xijiang, Z. Research on Drag Reduction Effect of Concave Non-smooth Surface in Air. *Adv. Mater. Res.* **2011**, *299–300*, 7–11.
20. Yan, F.; Yang, H.; Wang, L. Study of the Drag Reduction Characteristics of Circular Cylinder with Dimpled Surface. *Water* **2021**, *13*, 197. [[CrossRef](#)]
21. Shaughnessy, E.J.; Katz, I.M.; Schaffer, J.P. 8.4 Static, Dynamic, Stagnation and Total Pressure. In *Introduction to Fluid Mechanics*; Oxford University Press: New York, NY, USA, 2005; pp. 490–491.
22. Barker, G. *The Engineer's Guide to Plant Layout and Piping Design for the Oil and Gas Industries*; Gulf Professional Publishing: Burlington, MA, USA, 2018.
23. Genium Publishing Corporation. 402.1—Guidelines for the Use of Data in Section 402. In *Fluid Flow—Data Book*; Genium Publishing Corporation: New York, NY, USA, 1993; p. 5.
24. Layton, W. 5.4 The Reynolds Number. In *Introduction to the Numerical Analysis of Incompressible Viscous Flows*; Society for Industrial and Applied Mathematics: Philadelphia, PA, USA, 2008; pp. 83–86.
25. Vafadar, A.; Guzzomi, F.G.; Hayward, K. Experimental Investigation and Comparison of the Thermal Performance of Additively and Conventionally Manufactured Heat Exchangers. *Metals* **2021**, *11*, 574. [[CrossRef](#)]
26. Çengel, Y.A.; Cimbala, J.M. Chapter 10—Approximate Solutions of the Navier-Stokes Equations: Turbulent Flat Plate Boundary Layer. In *Fluid Mechanics: Fundamentals and Applications*; McGraw-Hill Higher Education: New York, NY, USA, 2017; p. 1117.
27. Ting, L.L. Effects of Dimple Size and Depth on Golf Ball Aerodynamic Performance. In Proceedings of the ASME/JSME 2003 4th Joint Fluids Summer Engineering Conference, Honolulu, HI, USA, 6–10 July 2009.
28. Schuetz, T. 4.3.1 Pressure and Friction Drag. In *Aerodynamics of Road Vehicles*; SAE International: Pittsburgh, PA, USA, 2016; pp. 220–221.
29. Chowdhury, H.; Loganathan, B.; Wang, Y.; Mustary, I.; Alam, F. A study of dimple characteristics on golf ball drag. *Procedia Eng.* **2016**, *147*, 87–91. [[CrossRef](#)]
30. Ge, M.-w.; Fang, L.; Liu, Y.-q. Drag reduction of wall bounded incompressible turbulent flow based on active dimples/pimples. *J. Hydrodyn.* **2017**, *29*, 261–271. [[CrossRef](#)]
31. Chanson, H. *Hydraulics of Open Channel Flow*; Butterworth Heinemann: Oxford, UK, 2004.
32. Choi, J.; Jeon, W.-P.; Choi, H. Mechanism of drag reduction by dimples on a sphere. *Phys. Fluids* **2006**, *18*, 041702. [[CrossRef](#)]
33. Patel, I.H.; Borse, S.L. Experimental Investigation of Heat Transfer Enhancement over the Dimpled Surface. *Int. J. Eng. Sci. Technol.* **2012**, *4*, 3666–3672.